Mon. Not. R. Astron. Soc. **387,** 729–734 (2008) doi:10.1111/j.1365-2966.2008.13256.x

Periodicity search for possible X-ray counterparts to radio-quiet gamma-ray pulsar candidates

Lupin Chun-Che Lin and Hsiang-Kuang Chang★
Department of Physics and Institute of Astronomy, National Tsing Hua University, Hsinchu 30013, Taiwan

Accepted 2008 March 25. Received 2008 March 14; in original form 2007 November 27

ABSTRACT

A periodicity search of gamma-ray data is usually difficult because of the small number of detected photons. A periodicity in the timing signal at other energy bands from the counterpart to the gamma-ray source may help to establish the periodicity in the gamma-ray emission and strengthen the identification of the source in different energy bands. However, it may still be difficult to find the period directly from X-ray data because of limited exposure. We have developed a procedure, by cross-checking two X-ray data sets, to find candidate periods for X-ray sources that are possible counterparts to gamma-ray pulsar candidates. Here, we report on the results of this method obtained with all the currently available X-ray data of eight X-ray sources. Some attractive periodicity features were found. These candidate periods can serve as the target periods for a future search when new data become available, so that a blind search with a huge number of trials can be avoided.

Key words: stars: neutron – pulsars: general – gamma-rays: observations – X-rays: general.

1 INTRODUCTION

There is not yet a good understanding of the electrodynamics in the magnetosphere of a neutron star, although fascinating phenomena, as revealed in emissions across the whole electromagetic spectrum from neutron stars, have been observed for 40 years. Among the 2000 or so radio pulsars catalogued to date, only seven have been detected at photon energies higher than 100 MeV and three more have been detected at a lower confidence level (Thompson 2004). These seven include Geminga, which does not emit radio waves or emits only at a very low level (Kuz'min & Losovskii 1999). The effort to understand gamma-ray emissions from pulsars has resulted in two types of model: the slot-gap model (Muslimov & Harding 2004) and the outer-gap model (e.g. Cheng, Ruderman & Zhang 2000; Hirotani 2007; Takata & Chang 2007). These models, although differing in the assumed emission site and mechanisms, have in many ways been successful in explaining pulse profiles and spectra. However, they do give different estimates of the fraction of radio-quiet gamma-ray pulsars, such as Geminga, among all the gamma-ray pulsars (Harding, Grenier & Gonthier 2007). A gamma-ray pulsar may be radio-quiet if its gamma-ray beam is wider than its radio beam or if these beams are in different directions. It is also possible that it is intrinsically weak in radio emission because of unfavoured spin periods and magnetic field strength. Although there is not yet a consistent model for radio emission from pulsars, several empirical models are available. Given a radio emission model (e.g. Johnston & Weisberg 2006), different models for gamma-ray pulsars may be discriminated by comparing their estimates of the radio-quiet gamma-ray pulsar fraction with observations, in addition to comparing their predictions of high-energy emission polarization characteristics (e.g. Takata, Chang & Cheng 2007).

There are only seven currently known gamma-ray pulsars, which is obviously too small a number to give a meaningful fraction for radio-quiet gamma-ray pulsars. With the launch of the *Gamma-Ray Large Area Space Telescope* (*GLAST*) and *AGILE*, the number of gamma-ray pulsars is expected to increase significantly. However, radio-quiet gamma-ray pulsars may still be difficult to find, mainly because of the limited amount of gamma-ray photons. It was only after Geminga's period was discovered in the *ROSAT* data (Halpern & Holt 1992) that its pulsation in gamma-rays was then found. Very often, it is also difficult to find the period in X-ray data, particularly when the data are sparse and a blind search over a large range of periods is performed. Efforts to find new radio-quiet gamma-ray pulsars from unidentified Energetic Gamma-Ray Experiment Telescope (EGRET) sources in a multiwavelength approach have not yet yielded definite results (e.g. Reimer et al. 2001; Halpern et al. 2002). Among the unidentified EGRET sources, many are at low galactic latitude and may be gamma-ray pulsars. Continuing this effort, we conducted a periodicity search for possible X-ray counterparts to some bright unidentified EGRET sources, using all available archival data and the method of cross-checking two data sets to look for candidate periods. The purpose of this cross-checking procedure is to find relatively significant signatures of possible pulsations occurring in two independent data sets. We report on the candidate periods and the corresponding period time derivatives found in this way, which can serve as the target periods to verify in future X-ray or gamma-ray data.

★E-mail: hkchang@phys.nthu.edu.tw

2 SOURCE SELECTION AND DATA REDUCTION

In an effort to understand the nature of unidentified EGRET sources, Roberts, Romani & Kawai (2001a) presented a catalogue of 2–10 keV *ASCA*/GIS images of fields containing 30 bright GeV sources. These GeV sources were selected from the brightest sources in the catalogue compiled by Lamb & Macomb (1997), using only photons with energies above 1 GeV from the EGRET public archives that incorporate the first 4.5 yr of the *Compton Gamma-Ray Observatory* (*CGRO*)/EGRET observations. Among these GeV sources, some are identified pulsars and quasars, some are possible counterparts to previously known objects, and others have not yet been identified as sources in other energy bands. Possible X-ray counterparts of these unidentified GeV sources were proposed in Roberts et al. (2001a). To search for new radio-quiet gamma-ray pulsars, we look for the periodicity of possible X-ray counterparts to those unidentified GeV sources, which have not yet been ruled out as possible gamma-ray pulsars. Furthermore, as explained in the next section, two data sets adequate for timing analysis are needed for the cross-checking method to find candidate periods. Six GeV sources among the 30 in the catalogue of Roberts et al. (2001a) were thus selected. One of the six sources (GeV J1417−6100) has four potential X-ray counterparts. Another one of the six sources (GeV J0008+7304) has been investigated with the same procedure described in this paper. The periodicity search result of its possible X-ray counterpart, RX J0007.0+7302, was reported by Lin & Chang (2005), and will not be repeated here. The eight X-ray sources and their data used in this study are listed in Table 1. Detailed descriptions of each GeV source can be found in Roberts et al. (2001a).

GeV J1417−6100 is in the direction of the 'Kookaburra' radio complex (Roberts et al. 1999). A 68-ms radio pulsar, PSR J1420−6048, was found at a position consistent with AX J1420.1−6049 (D'Amico et al. 2001), which is in the north-eastern wing of the Kookaburra. The pulsation at the radio period in X-rays was only marginally detected with *ASCA* data (Roberts, Romani & Johnston 2001b). *Chandra* images of AX J1420.1−6049 clearly show a compact source at the position of PSR J1420−6048, but its pulsation in X-rays at the radio period cannot be confirmed with the current *Chandra* data (Ng, Roberts & Romani 2005). The identification between PSR J1420−6048 and AX J1420.1−6049 is not yet conclusive. We therefore include AX J1420.1−6049 in our periodicity search. AX J1418.7−6058 is located in the south-western wing of the Kookaburra (the 'Rabbit'). Two compact sources denoted as 'R1' and 'R2' in the Rabbit were identified in *Chandra* and *XMM* images (Ng et al. 2005). Although 'R1' might be a background source, we have still used it as the target in the *XMM* data for cross-checking periodicity signatures with earlier *ASCA* and *BeppoSAX* data, as 'R1' is much brighter than 'R2' and in those earlier data photons from 'R1' dominate. More recently, two extended TeV sources (HESS J1420−607 and HESS J1418−609) were discovered, spatially coincident with the two wings of the Kookaburra (Aharonian et al. 2006). It is likely that 3EG J1420−6038 and GeV J1417−6100 are two separate sources associated with HESS J1420−607 and HESS

Table 1. List of data used in this study. Column 1 is the name of the X-ray source with its possible gamma-ray counterpart in parentheses. Column 2 is the instrument used to obtain the data. Column 3 is the data epoch (in MJD), which is the middle point in the whole data time-span. Columns 4 and 5 are the total exposure time and the total time-span of the data used. Both are in units of ks. Column 6 gives the target position, and column 7 gives the number of photons after extraction, the radius of the extraction circle and the extraction energy range (in keV) for the X-ray target under study. Column 8 is the sequence number labelling the data used in this work for later referencing.

(1)	(2)	(3)	(4)	(5)	(6)	(7)	(8)
AX J1418.2-6047	*ASCA*/GIS	50317.00727	25.6	106	($14^h18^m15^s.8$, $-60°46'44''$)	311; 90″; 1–10	01
(GeV J1417-6100)	*ASCA*/GIS	51223.68497	22.2	173	($14^h18^m15^s.8$, $-60°46'44''$)	126; 90″; 1–6	02
	BeppoSAX/MECS	52289.79012	30.8	51.0	($14^h18^m15^s.8$, $-60°46'44''$)	105; 120″; 2–10	03
AX J1418.6-6045	*ASCA*/GIS	50317.00727	25.6	106	($14^h18^m37^s.0$, $-60°45'12''$)	271; 90″; 1–8	04
(GeV J1417-6100)	*ASCA*/GIS	51223.68497	22.2	173	($14^h18^m37^s.0$, $-60°45'12''$)	133; 90″; 1–7	05
	BeppoSAX/MECS	52289.79013	30.8	51.0	($14^h18^m37^s.0$, $-60°45'12''$)	148; 120″; 2–10	06
AX J1418.7-6058	*ASCA*/GIS	50317.00728	25.6	106	($14^h18^m38^s.6$, $-60°57'49''$)	314; 90″; 1–8	07
(GeV J1417-6100)	*ASCA*/GIS	51223.68496	22.2	173	($14^h18^m38^s.6$, $-60°57'49''$)	551; 90″; 1–7	08
	BeppoSAX/MECS	52289.79050	30.8	51.0	($14^h18^m38^s.6$, $-60°57'49''$)	569; 210″; 2–10	09
	XMM/pn	52708.65941	26.9	26.9	($14^h18^m42^s.8$, $-60°58'03''.6$)	632; 15″; 0.2–12	10
AX J1420.1-6049	*ASCA*/GIS	50317.00729	25.6	106	($14^h20^m07^s.8$, $-60°48'56''$)	214; 90″; 1.5–8	11
(GeV J1417-6100)	*ASCA*/GIS	51223.68495	22.2	173	($14^h20^m07^s.8$, $-60°48'56''$)	252; 90″; 1.5–8	12
	BeppoSAX/MECS	52289.79017	30.8	51.0	($14^h20^m07^s.8$, $-60°48'56''$)	904; 210″; 2–10	13
	Chandra/ACIS	52534.12055	31.2	31.2	($14^h20^m08^s.2$, $-60°48'16''.9$)	229; 2″; 1–7	14
AX J1809.8-2332	*ASCA*/GIS	50526.78845	41.5	180	($18^h09^m48^s.6$, $-23°32'09''$)	1133; 90″; 0.8–7	15
(GeV J1809-2327)	*XMM*/pn	52539.07915	11.1	15.6	($18^h09^m50^s.0$, $-23°32'24''$)	542; 15″; 0.2–12	16
	XMM/pn	53280.71956	49.1	69.3	($18^h09^m50^s.0$, $-23°32'24''$)	4070; 15″; 0.2–12	17
AX J1836.2+5928	*ROSAT*/HRI	50800.00499	40.1	443	($18^h36^m13^s.6$, $+59°25'29''$)	224; 30″; 0.1–2.5	18
(GeV J1835+5921)	*Chandra*/HRC	53430.07235	45.2	45.2	($18^h36^m13^s.7$, $+59°25'30''$)	278; 1″; 0.08–10	19
	Chandra/HRC	53438.80937	28.1	28.1	($18^h36^m13^s.7$, $+59°25'30''$)	181; 1″; 0.08–10	20
	Chandra/HRC	53440.60818	45.2	45.2	($18^h36^m13^s.7$, $+59°25'30''$)	247; 1″; 0.08–10	21
AX J1837.5-0610	*ASCA*/GIS	50905.53135	19.7	37.0	($18^h37^m29^s.0$, $-06°09'38''$)	243; 90″; 1–9	22
(GeV J1837-0610)	*ASCA*/GIS	51105.10478	17.9	40.0	($18^h37^m29^s.0$, $-06°09'38''$)	203; 90″; 1–9	23
	BeppoSAX/MECS	51981.25968	40.2	94.5	($18^h37^m32^s.5$, $-06°09'49''$)	739; 210″; 2–10	24
	BeppoSAX/MECS	52016.65630	42.7	105	($18^h37^m32^s.5$, $-06°09'49''$)	770; 210″; 2–10	25
AX J2021.1+3651	*ASCA*/GIS	51300.06891	21.8	69.8	($20^h21^m07^s.8$, $+36°51'19''$)	294; 90″; 1–7	26
(GeV J2020+3658)	*Chandra*/ACIS	52682.60172	20.8	20.8	($20^h21^m05^s.5$, $+36°51'04''.8$)	575; 1″; 0.2–5	27

J1418−609, respectively (Aharonian et al. 2006). Another two X-ray sources, AX J1418.2−6047 and AX J1418.6−6045, denoted as 'Src2' and 'Src3' in Roberts et al. (2001a), are both located in the 95 per cent error contour of GeV J1417−6100 and in the 99 per cent contour of 3EG J1420−6038 (Aharonian et al. 2006).

AX J1809.8−2332 is the brightest X-ray source within the 99 per cent error box of GeV J1809−2327 (3EG J1809−2328). *Chandra* images of this region reveal a point X-ray source connected to a non-thermal X-ray/radio nebula (Braje et al. 2002). *XMM* images show a larger, broader X-ray emission region with a ridge of emission along the symmetric axis of the radio nebula (Roberts et al. 2006). The X-ray point source is very likely a pulsar moving at the tip of its associated pulsar wind nebula. It would be very desirable to find its pulsation period.

GeV J1835+5921 and its possible X-ray counterpart AX J1836.2+5928 have long been considered as the next Geminga to find. Strong evidence from *Chandra* and *Hubble Space Telescope* (*HST*) observations indicates that AX J1836.2+5928 (RX J1836.2+5925) is a neutron star (Halpern et al. 2002). Using the *Chandra* data listed in Table 1, Halpern, Camilo & Gotthelf (2007) reported on unsuccessful searches for pulsations from RX J1836.2+5925 in the period range from 1 ms to 10 s and a pulsed-fraction upper limit of 35 per cent.

There are fewer observations of the GeV J1837−0610 region. A 96-ms radio pulsar (PSR J1837−0604) was discovered and it was suggested that this was associated with GeV J1837−0610 (3EG J1837−0606; D'Amico et al. 2001). However, the position of PSR J1837−0604 is at the rim of the 95 per cent confidence contour of GeV J1837−0610 and is inconsistent with AX J1837.5−0610, which is the single X-ray point source within the 95 per cent confidence contour of GeV J1837−0610 in *ASCA* images.

Chandra observations of AX J2021.1+3651 (Hessels et al. 2004) indicate that this X-ray source is a pulsar wind nebula and that there is an X-ray point source located at the centre of this nebula, where a 104-ms radio pulsar (PSR J2021+3651) was found (Roberts et al. 2002). The X-ray pulsation of this point source at the radio period was only marginally found in the *Chandra* data with an *H*-test score of 11.7 (Hessels et al. 2004).

All the data were processed with standard procedures as outlined below. Photons for timing analysis were selected within a circle around the target and within a certain energy range. The circle radii and energy-range boundaries were chosen so that the target contribution was clearly detected. The target positions, the radii of the circles and the energy ranges adopted in this work are listed in Table 1. All the photon arrival times were corrected to the solar system barycentre. The corrected time list was then used for timing analysis to look for periodicity.

3 CROSS-CHECKING METHOD FOR PERIODICITY SEARCH

Photon-counting coherent-timing methods are usually used for a periodicity search in sparse data (i.e. each photon arrival time is converted to a phase value with a given period and its time derivatives). The distribution of these phase values is then tested against the null hypothesis with a certain statistical method to assess the probability that the observed distribution is consistent with a statistically flat distribution. In this work, we adopted the *H*-test (De Jager, Swanepoel & Raubenheimer 1989; De Jager 1994) as the method to assess the random probability.

The difficulty in finding the period in sparse data, in addition to the limited number of observations, is that a blind search with a huge number of trial periods (and period time derivatives) is unavoidable if an a priori period or period range is not known. When the total number of independent trials is taken into account, a significantly low random probability is seldom obtained. One possible way to improve upon this is to cross-check two different data sets to look for possible support for the reality of an attractive candidate period found in one data set.

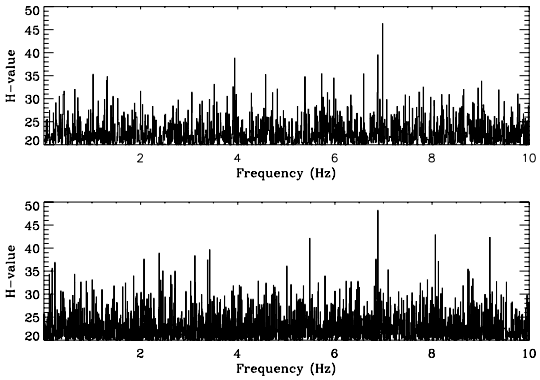

Figure 1. Examples of *H*-test blind search results, for AX J1420.1−6049 with data sets 11 and 12 (see Table 1). The number of independent trial frequencies is about 10^6 for each case. Most of the trials yield a very low *H*-value. Only *H*-values larger than 20 are plotted.

For each of the X-ray sources discussed in the previous section, we first performed a blind search in every available data set of that source. Depending on the time resolution of the data, different search ranges were chosen for the trial periods. For all the *ASCA*/GIS data, the search range is from 0.1 to 100 s. For all the others, it is from 0.01 to 100 s. Because each data set spans a relatively short time, we constrained ourselves at this stage to considering trial periods only without their time derivatives. This makes it a one-dimensional search. We chose the searching step to be a small fraction (typically 1/5) of the corresponding independent Fourier spacing, which is P^2/T in the period domain ($1/T$ in frequency), where P is the trial period and T is the total time-span of the data. A blind search usually has several attractive features. One example is shown in Fig. 1. For the convenience of the reader, in Fig. 2 we plot the random probability for a single trial to have an *H*-value larger than a certain number.

From the result of a blind search in a certain data set, a few trial periods with high *H*-values were picked out for cross-checking. This number of such trial periods is obviously arbitrary. We picked out

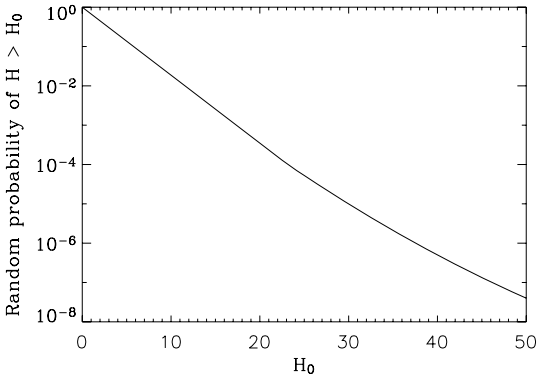

Figure 2. The *H*-test probability distribution (De Jager et al. 1989). The plotted curve is the null hypothesis random probability for a single trial to have an *H*-value larger than H_0.

the top five in this work. Each of these five usually has a significantly low random probability if the total number of independent trials in the blind search is not taken into account. As mentioned above, a blind search has a huge number of independent trials, typically more than 10^6. Therefore, for each of these, we look for possible associated features in other data sets to assess its reality. To do this, we set two further criteria. First, we look for associated features of the H-test results in another data set only within the range that gives a corresponding characteristic age ($P/2\dot{P}$) larger than 1000 yr. A neutron star younger than that age would probably have a record in human history. In determining this range, the uncertainty of the period is estimated based on the method described in Leahy (1987). Secondly, the most prominent features in this range are identified, and the resulting random probability is calculated, which is the product of the random probability of the feature in the first data set and that of the feature in the second data set. When calculating the random probability of the feature in the second data set, only independent trials within the range specified by the first criterion are considered. Oversampling was not taken into account in our computation of the random probability. We keep only those cases whose resulting random probability is less than 0.01. The periods and the corresponding period time derivatives for these cases are listed in Table 2. The probability threshold of 0.01 is arbitrary. Of course, a higher random probability gives more candidate periods, but with less significance. Two examples of such an association are shown in Figs 3 and 4.

In data set 07, the candidate period of AX J1418.7−6058 at 0.10171064 s has an H-value of 56.7, which has a very low random probability for a single trial. With our procedure, there will be candidate periods satisfying our criteria in all the data sets 08, 09 and 10. Here we only report on the most significant. Its random probability, listed in Table 2, was derived using an H-value equal to 50 instead of 56.7, as in De Jager et al. (1989) the single trial random probability was provided only up to $H = 50$. Two similar cases are the candidate period at 0.014799899 s for AX J1420.1−6049, which has an H-value of 53.8 in data set 14, and that at 0.13247455 s for AX J1809.8−2332, which has an H-value of 59.5 in data set 15. Although in our procedure only the most prominent feature in the cross-checking window is picked out for association, for the candidate period of AX J1418.7−6058 at 0.10139550 s in data set 07, the association with the period of the second highest H-value in the cross-checking window of data set 09 is also reported here, as it is very close to the candidate period in data set 07 and its H-value is not too different from the highest. This association is shown in Fig. 5. The two candidate periods of AX J1809.8−2332 listed in Table 2 are related to each other. Based on their pulse profiles, we suggest the period at 0.13247455 s to be the second harmonic of that at 0.264949 s if they are real. In such a case, the derived period

Table 2. Candidate periods. Column 1 is the candidate period (in s) obtained from cross-checking the two data sets listed in column 7. The number in parentheses is the 1σ uncertainty to the last digit, estimated with the method described in Leahy (1987). The numbers followed by a triangle (△) are candidate periods favoured by examining the consistency with properties of currently known gamma-ray pulsars, as discussed in Section 4. The epoch (MJD) of this period is listed in column 5, which is the epoch of the data set containing the stronger signature for pulsation in the two data sets. Columns 2, 3 and 4 are the corresponding period time derivative (in units of 10^{-13} s s^{-1}), characteristic age (in yr) and spin-down power (in units of 10^{36} erg s^{-1}). Column 6 is the resultant random probability, as explained in the text.

	(1)	(2)	(3)	(4)	(5)	(6)	(7)
AX J1418.2−6047	0.2029690(1) △	2.00(4)	16 000	9.4(2)	50317.00727	4.7×10^{-3}	01, 03
	0.3097181(5)	47.3(1)	1000	6.29(1)	51223.68497	2.7×10^{-3}	01, 02
	0.4289840(5)	33.6(1)	2000	1.682(6)	51223.68497	5.3×10^{-3}	01, 02
AX J1418.6–6045	0.12180376(5)	6.65(2)	2900	14.51(4)	51223.68497	9.1×10^{-3}	05, 06
	0.15935800(7) △	2.01(1)	12 500	1.96(1)	50317.00727	5.3×10^{-3}	04, 05
	0.3311744(5)	39.39(9)	1300	4.275(9)	50317.00727	2.7×10^{-3}	04, 05
	0.3311744(5)	31.04(6)	1700	3.366(7)	50317.00727	3.2×10^{-4}	04, 06
AX J1418.7–6058	0.10139550(2)	0.080(4)	200 000	0.30(2)	50317.00728	9.6×10^{-3}	07, 09
	0.10139550(2)	7.757(5)	2100	29.32(2)	50317.00728	3.6×10^{-3}	07, 09
	0.10171064(5)	9.337(6)	1700	34.95(2)	50317.00728	$<3.9 \times 10^{-3}$	07, 09
	0.10969281(4)	14.45(1)	1200	43.03(3)	50317.00728	4.2×10^{-3}	07, 10
	0.1443257(1)	18.35(2)	1250	24.13(2)	51223.68496	1.9×10^{-4}	07, 08
	0.3274125(3)	31.29(8)	1650	3.515(9)	51223.68496	9.5×10^{-3}	08, 09
AX J1420.1–6049	0.014799899(6)	0.392(3)	6000	478(4)	52534.12055	$<6.2 \times 10^{-3}$	13, 14
	0.019576788(3)	2.616(3)	1200	1376(1)	52289.79017	7.2×10^{-3}	13, 14
	0.033549387(8)	0.133(7)	40 000	13.9(8)	52289.79017	1.2×10^{-3}	13, 14
	0.14526767(4)	4.84(2)	4750	6.24(2)	51223.68495	4.1×10^{-5}	11, 12
	0.14526767(4) △	1.35(3)	17 000	1.74(3)	51223.68495	5.0×10^{-3}	12, 13
	0.1881326(4)	10.1(3)	2900	6.0(2)	52534.12055	3.8×10^{-3}	13, 14
	0.2540350(5)	13.17(7)	3100	3.17(2)	50317.00729	5.0×10^{-3}	11, 12
AX J1809.8–2332	0.13247455(3)	16.439(5)	1300	27.792(8)	50526.78845	$<1.9 \times 10^{-2}$	15, 17
	0.2649491(2)	27.4(1)	1500	5.80(2)	50526.78845	7.4×10^{-4}	15, 16
AX J1836.2+5928	0.022425706(5)	0.77(9)	5000	$2.7(3) \times 10^2$	53440.60818	6.5×10^{-3}	19, 21
	0.03350910(2)	2(2)	2000	$2(2) \times 10^2$	53438.80937	5.3×10^{-3}	20, 21
	0.034677614(1)	0.0201(4)	270 000	1.90(4)	50800.00499	5.5×10^{-3}	18, 19
	0.1679234(4) △	0.16(2)	170 000	0.13(1)	53440.60818	9.1×10^{-3}	18, 21
AX J1837.5–0610	0.1736610(3)	18.6(5)	1500	14.0(3)	51105.10478	2.8×10^{-3}	22, 23
AX J2021.1+3651	None						

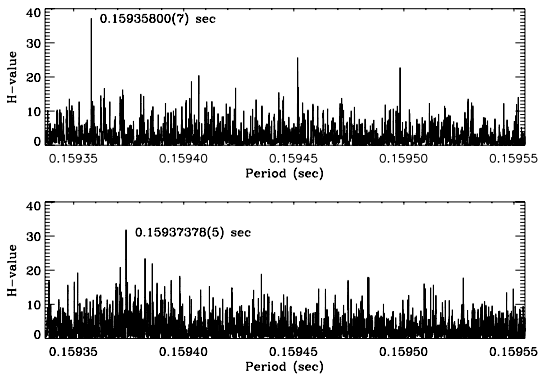

Figure 3. The identification of the candidate period at 159 ms for AX J1418.6−6045 using data sets 04 and 05. The trial period range shown in the lower panel of this figure (from data set 05) is roughly the range specified by the criterion that the corresponding characteristic age is larger than 1000 yr if a possible period is to be associated with that in the upper panel. The most significant feature in this range is at 0.15937378 s, and its association with that at 0.15935800 s in the upper panel yields a resultant random probability of 5.3×10^{-3}. We list all such cases with a random probability lower than 0.01 as a candidate period in Table 2.

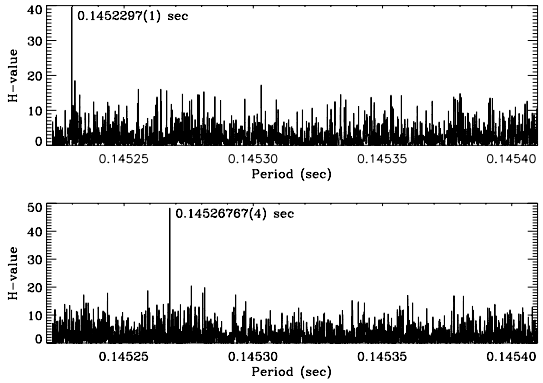

Figure 4. The identification of the candidate period at 145 ms for AX J1420.1−6049 using data sets 11 and 12. As in Fig. 3, the trial period range shown is roughly the range specified by the criterion that the characteristic age is larger than 1000 yr. This figure is in fact an enlarged view of Fig. 1 around 6.88564 Hz but plotted in the period domain. This example, with a resultant random probability of 4.1×10^{-5}, is the most significant signature found in this study.

derivative, characteristic age and spin-down power for the association between periodicity signatures found in data sets 15 and 17 near 0.1325 s will be 2, 1 and 0.25 times those listed in Table 2, respectively. This makes this association even more unfavourable if we compare its spin-down power with that of the Crab pulsar (see the discussion in the next section). However, the strong periodicity signature (Fig. 6) makes the candidate period at 0.264949 s very attractive.

To examine whether the procedure described above is useful, we applied it to the case of RX J1856.5−3754, whose X-ray emission is believed to be thermal emission from the surface of a neutron star. There were several *XMM* observations of this source, but no periodicity was found until Tiengo & Mereghetti (2007) reported a period of 7.055 s with a random probability of 6×10^{-4}. This result was obtained by analysing the *XMM* data taken in 2006 October. Applying our cross-checking method as described above to previous data, we found that the 7-s period was also chosen and suggested as

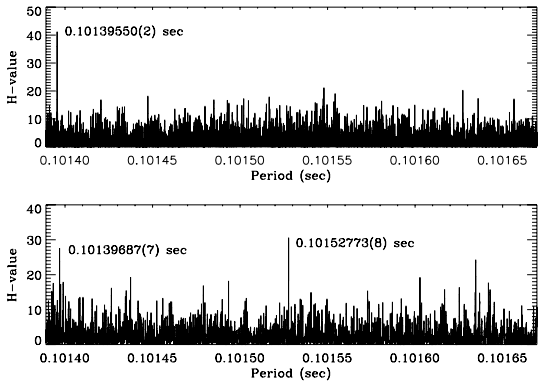

Figure 5. The identification of the candidate period at 101.4 ms for AX J1418.7−6058 using data sets 07 and 09. As in Figs 3 and 4, the trial period range shown in the lower panel is roughly the range specified by the criterion that the characteristic age is larger than 1000 yr. The two possible period associations, which result in different period time derivatives, are both included in Table 2.

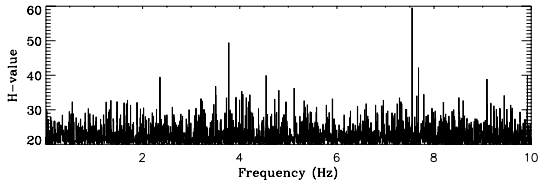

Figure 6. The *H*-test blind search results of AX J1809.8−2332 with data set 15. The two highest features correspond to periods at 0.13247455 and 0.2649491 s respectively.

a candidate period. This demonstrates, although does not guarantee, the usefulness of our cross-checking method.

4 DISCUSSION

We applied the periodicity cross-checking procedure described in Section 3 to the eight X-ray sources listed in Table 1. Candidate periods obtained with this method are listed in Table 2. Future periodicity searches of X-rays or gamma-rays may be conducted around these candidate periods, instead of performing blind searches. Among all these candidate periods, that with the lowest random probability (4.1×10^{-5}) is 145.2297 ms for AX J1420.1−6049. Its implied characteristic age, 4800 yr, is between those of the Crab and Vela pulsars. However, its corresponding spin-down power is similar to that of the Vela pulsar, which in turn is about 100 times smaller than that of the Crab pulsar. If there is a correlation between the characteristic age and the spin-down power, this candidate period is not favourable, because its associated spin-down power is too small for its 4800-yr characteristic age.

Indeed, among the currently known gamma-ray pulsars, the spin-down power decreases with increasing characteristic age. The Crab, Vela and Geminga pulsars have characteristic ages of $10^{3.1}$, $10^{4.1}$ and $10^{5.5}$ yr, and spin-down powers of $10^{38.7}$, $10^{36.8}$ and $10^{34.5}$ erg s^{-1}, respectively. Thus, one possible way to further assess the reality of these candidate periods is to compare their corresponding properties, such as the characteristic age and spin-down power, with those of known gamma-ray pulsars. Along this line of thinking, the candidate periods at 203 ms for AX J1418.2−6047, at 159 ms for AX J1418.6−6045, at 19.6 and 145 ms for AX J1420.1−6049, and at 22.4, 33.5 and 168 ms for AX J1836.2+5928 are favoured.

This is because their corresponding characteristic ages and spin-down powers are roughly consistent with those of known gamma-ray pulsars.

Another property to consider is the X-ray to gamma-ray energy spectral index, defined in Roberts et al. (2001a), which assumes an X-ray counterpart to those unidentified GeV sources and leads to three X-ray brightness categories for the GeV sources under study. In this scheme, the Crab pulsar is X-ray bright, the Vela pulsar is X-ray moderate and Geminga is X-ray faint. The GeV sources associated with the aforementioned X-ray sources are all X-ray moderate (similar to Vela), except for GeV J1835+5921, which is X-ray faint (similar to Geminga). Examining the characteristic ages, we note that the four candidate periods at 203 ms for AX J1418.2−6047, at 159 ms for AX J1418.6−6045, at 145 ms for AX J1420.1−6049 and at 168 ms for AX J1836.2+5928 survive the comparison. The candidate period at 127.5 ms for RX J0007.0+7302, reported by Lin & Chang (2005), is also supported by these comparisons.

These five X-ray sources are possible counterparts to three (or four) GeV sources: GeV J0008+7304, GeV J1417−6100 (or a probable separate source 3EG J1420−6038) and GeV J1835+5921. For the former two (or three), if the candidate periods suggested here are true, they will be more Vela-like, in terms of timing properties. This would suggest that the major cause for a gamma-ray pulsar to be radio-quiet is likely geometrical, rather than intrinsic. Also, the gamma-ray beam is wider than the radio beam so, for a certain viewing angle, both the radio and gamma-ray emissions are observed, as in the case of Vela, and in another viewing angle only the gamma-ray emission is observed. Instead, if all the radio-quiet gamma-ray pulsars are similar to Geminga in their timing properties, the reason for being radio-quiet, although not yet clear, is probably intrinsic.

The timing properties of undiscovered gamma-ray pulsars may not be similar to those already known, particularly because the number of gamma-ray pulsars that have been discovered is still small. Thus, all the candidate periods listed in Table 2 may still be helpful for pinning down the periodicity of emissions from these sources in the future, when new X-ray or gamma-ray data obtained with *AGILE* and *GLAST* become available. A larger sample of gamma-ray pulsars, either radio-loud or radio-quiet, will help us to understand better the radiation mechanisms in the magnetospheres of gamma-ray pulsars.

ACKNOWLEDGMENTS

This research has made use of data obtained through the High Energy Astrophysics Science Archive Research Centre Online Service, provided by the NASA/Goddard Space Flight Centre. This work was supported by the National Science Council and the National Space Organization of the Republic of China through grants NSC 96-2628-M-007-012-MY3 and 96-NSPO(B)-SP-FA04-01.

REFERENCES

Aharonian F. et al., 2006, A&A, 456, 245
Braje T. M., Romani R. W., Roberts M. S. E., Kawai N., 2002, ApJ, 565, L91
Cheng K. S., Ruderman M., Zhang L., 2000, ApJ, 537, 964
D'Amico N. et al., 2001, ApJ, 552, L45
De Jager O. C., 1994, ApJ, 436, 239
De Jager O. C., Swanepoel J. W. H., Raubenheimer B. C., 1989, A&A, 221, 180
Halpern J. P., Holt S. S., 1992, Nat, 357, 222
Halpern J. P., Gotthelf E. V., Mirabal N., Camilo F., 2002, ApJ, 573, L41
Halpern J. P., Camilo F., Gotthelf E. V., 2007, ApJ, 668, 1154
Harding A. K., Grenier I. A., Gonthier P. L., 2007, Ap&SS, 309, 221
Hessels J. W. T., Roberts M. S. E., Ransom S. M., Kaspi V. M., Romani R. W., Ng C.-Y., Freire P. C. C., Gaensler B. M., 2004, ApJ, 612, 389
Hirotani K., 2007, ApJ, 662, 1173
Johnston S., Weisberg J. M., 2006, MNRAS, 368, 1856
Kuz'min A. D., Losovskii B. Y., 1999, Astron. Lett., 25, 80
Lamb R. C., Macomb D. J., 1997, ApJ, 488, 872
Leahy D. A., 1987, A&A, 180, 275
Lin L. C.-C., Chang H.-K., 2005, Ap&SS, 297, 361
Muslimov A. G., Harding A. K., 2004, ApJ, 606, 1143
Ng C.-Y., Roberts M. S. E., Romani R. W., 2005, ApJ, 627, 904
Reimer O., Brazier K. T. S., Carramiñana A., Kanbach G., Nolan P. L., Thompson D. J., 2001, MNRAS, 324, 772
Roberts M. S. E., Romani R. W., Johnston S., Green A. J., 1999, ApJ, 515, 712
Roberts M. S. E., Romani R. W., Kawai N., 2001a, ApJS, 133, 451
Roberts M. S. E., Romani R. W., Johnston S., 2001b, ApJ, 561, L187
Roberts M. S. E., Hessels J. W. T., Ransom S. M., Kaspi V. M., Freire P. C. C., Crawford F., Lorimer D. R., 2002, ApJ, 577, L19
Roberts M. S. E., Gotthelf E. V., Halpern J. P., Brogan C. L., Ransom S. M., 2006, in Becker W., Huang H.-H., eds, MPE Report 291, Proc. 363 WE-Heraeus Seminar on Neutron Stars and Pulsars. Max-Planck Institute für extraterrestrische Physik, Garching, p. 24 (astro-ph/0612631v1)
Takata J., Chang H.-K., 2007, ApJ, 670, 677
Takata J., Chang H.-K., Cheng K. S., 2007, ApJ, 656, 1044
Thompson D. J., 2004, in Cheng K. S., Romero G. E., eds, Cosmic Gamma-Ray Sources. Kluwer, Dordrecht, p. 149
Tiengo A., Mereghetti S., 2007, ApJ, 657, L101

This paper has been typeset from a TEX/LATEX file prepared by the author.